Radiation Physics and Chemistry 199 (2022) 110343

Contents lists available at ScienceDirect

Radiation Physics and Chemistry

journal homepage: www.elsevier.com/locate/radphyschem

Synergistic effect of e-beam irradiation and graphene oxide incorporation on thermal, mechanical, and barrier properties of poly (ethylene-co-vinyl alcohol) film

Julyana G. Santana [a], Meshude Akbulut [b], Marcia L.A. Temperini [c], Vijay K. Rangari [d], Olgun Güven [b], Esperidiana Moura [a,*]

[a] Centro de Química e Meio Ambiente, Instituto de Pesquisas Energéticas e Nucleares, Av. Prof. Lineu Prestes, 2242, São Paulo, 05508-000, SP, Brazil
[b] Hacettepe University, Department of Chemistry, Polymer Chemistry Division, Beytepe, Ankara, 06800, Turkey
[c] Departamento de Química Fundamental, Instituto de Química, Universidade de São Paulo, Av. Prof. Lineu Prestes, 748, São Paulo, 05508-000, SP, Brazil
[d] Department of Materials Science and Engineering, Tuskegee University, Tuskegee, AL, USA

ARTICLE INFO

Keywords:
EVOH/GO films
e-beam irradiation
Tensile properties
Barrier properties
Morphology
FEG-SEM
TEM

ABSTRACT

Graphene and its derivatives, such as graphene oxide (GO), have attracted enormous interest from academia and industry because of its unique electrical, mechanical, and thermal properties, which can lead to enhanced material performance. In the present study, low contents of GO were incorporated into the poly (vinyl alcohol-co-ethylene) (EVOH). First, the GO was prepared by chemical oxidation of graphite employing a modified Hummer's method. The GO content of 0.1–0.3 wt % was incorporated in the EVOH matrix using a twin-screw extruder and extrusion blown film process to prepare flexible films. EVOH/GO film samples were irradiated at 100 kGy, using a 1.5 MeV electron-beam accelerator, at room temperature, in the presence of air. GO was characterized by XRD, ATR-FTIR, FE-SEM, and TEM analysis. XRD patterns of GO show a sharp reflection peak at $2\theta = 10^{\circ}$ (d001) corresponding to a d-spacing at 8.84 Å, characteristic of GO. The non-irradiated and irradiated samples were characterized by XRD, FEG-SEM, TG, DSC, oxygen transmission rate (OTR), UV/VIS analysis, and tensile tests. EVOH/GO nanocomposite films had an improved oxygen barrier, while also retaining fairly good transparency. As an effect of e-beam irradiation, the thermal, mechanical, and barrier behaviors of the nanocomposite films were even better than non-irradiated film samples, and obviously better than neat EVOH. Thus, the incorporation of low contents of GO followed by e-beam radiation treatment might be an interesting alternative to produce packaging materials based on EVOH with outstanding performance even under very humid conditions.

1. Introduction

Currently, flexible packaging is widely used for food packaging applications instead of rigid packaging. Flexible plastics are thin, light, easily stretchable, chemically inert, and attractive. Due to the smaller amount of resin required for its manufacturing, it is cost-effective compared to rigid packaging. These characteristics emphasize the brand appeal of the packaged food product. Flexible food packaging should have good gas and vapor barrier properties to protect the food from the external environment, to prevent the deterioration by oxidation and discoloration, and to avoid texture and nutrient loss of the components. In addition to the good barrier, mechanical strength, heat resistance, puncture resistance, chemical resistance, transparency, gloss, and printability are also required properties.

The various characteristics required for flexible food packaging can be achieved by lamination or co-extrusion with metal foil and other layers with different polymers for specific functions depending on the food and the intended shelf life (Coles et al., 2003; Raheem, 2013; Marsh and Bugusu, 2007; Mokwena and Tang, 2012). Polyethylenes and polypropylenes (homo- and copolymers) are used for contact with the product because of their excellent chemical resistance and inertness to most foods, good barrier against water, and thermostability. Polyethylene terephthalate (PET) has good tensile and yield strength as well as being transparent after processing. Polyamides offer good chemical

* Corresponding author.
E-mail address: eabmoura@ipen.br (E. Moura).

https://doi.org/10.1016/j.radphyschem.2022.110343
Received 1 December 2021; Received in revised form 29 April 2022; Accepted 17 June 2022
Available online 21 June 2022

resistance, toughness, and low gas permeability. Poly (vinyl alcohol-co-ethylene) (EVOH) has one of the lowest oxygen permeability reported among polymers used in flexible packaging (Marsh and Bugusu, 2007; Mokwena and Tang, 2012; Cui et al., 2016).

EVOH are a family of resins with excellent gas-barrier properties. EVOH resins with a copolymerization ratio between 25 and 45 mol % of ethylene have superior gas-barrier properties than most polymeric materials. EVOH resins are widely used in the food packaging industry, due to their exceptional gas-barrier properties to oxygen and organic compounds, and low absorption rate of odor and flavor. EVOH also has excellent resistance to oils and organic solvents, substantial chemical resistance, high transparency, and easy processability on a wide range of conventional co-extrusion processing equipment. Packaging with EVOH content for the gas-barrier layer is used to pack oily foods like potato chips, sausage, ham, and mineral oils, and even organic solvents and agricultural chemicals (Cui et al., 2016; Cabedo et al., 2006; Kucukpinar and Doruker, 2004).

However, EVOH at high relative humidity presents high water absorption, which can greatly affect its high gas barrier as well as its thermal and mechanical properties (Cui et al., 2016; Lasagab á ster et al., 2009; Kim et al., 2004; Mokwena et al., 2009). Studies have reported that the inclusion of impermeable lamellar fillers, such as clay and graphene, into EVOH with sufficient aspect ratio, can significantly enhance the gas-barrier properties of the polymer. The high aspect ratio of these nanofillers makes the gas diffusing molecules follow longer and more tortuous pathways to pass through the nanocomposite film (Cui et al., 2016; Arora and Padua, 2010; Bumbudsanpharoke and Ko, 2015; Kim et al., 2014a; Kim and Choi, 2015; Yang et al., 2013a).

Graphene and its derivatives, including graphene oxide (GO), have attracted attention because they exhibit remarkable and unusual gas impermeability, high optical transmittance, thermal conductivity, chemical stability, and excellent mechanical and electrical properties. Prepared from chemical oxidation of graphite, GO contains a range of reactive oxygen functional groups (Kim and Choi, 2015; Yang et al., 2013a; Yoo et al., 2014). One of the most promising applications of GO is in nanocomposites based on the polar polymer matrix. The increased interfacial adhesion between GO and polar polymer matrix facilitates exfoliated structure and homogeneous dispersion (Yang et al., 2013a; Yoo et al., 2014; Kim and Lee, 2014). Due to its gas-barrier performance as well as thermal and mechanical properties, GO has been incorporated into various thermoplastic polymers, including polyurethane, poly (methyl methacrylate), polyethylene, polystyrene, poly (vinyl alcohol), polyethylene terephthalate, poly (ethylene vinyl alcohol), and poly (lactic acid) (Yoo et al., 2014; Kim and Lee, 2014; Huang et al., 2012; Kim and Jeong, 2010; Al-Jabareen et al., 2012).

In this study, a small amount of graphene oxide was incorporated into EVOH by melt processing, and its effects on morphology, optical transparency, mechanical resistance, and oxygen barrier were evaluated in the EVOH/GO nanocomposite films. The principal aim of this work was to investigate the impact of incorporating GO to produce a high-performance composite film based on EVOH resin for food packaging applications and to explore the possibility of improving composite mechanical and oxygen barrier performances using e-beam radiation. The e-beam radiation was applied in this work because e-beam radiation processing is an excellent technique to adjust material surface properties as reported by the literature (Riganakos et al., 1999; El-Saftawy et al., 2018; Chen et al., 2020; Kim et al., 2005; Pramanik et al., 2014). Furthermore, our previous work found that EB irradiation induced changes in many physicochemical properties of EVOH, providing, among other desirable changes, improved mechanical properties (Oliveira et al., 2009; Moura et al., 2009; Santana et al., 2017). The effects of e-beam irradiation on EVOH/GO nanocomposite films were evaluated by comparing the results of irradiated samples with non-irradiated ones.

2. Experimental

2.1. Materials

Graphite flakes from Quimesp Química Ltda (São Paulo, Brazil); sulfuric acid (H_2SO_4, 98%); phosphoric acid (H_3PO_4, 85%); potassium permanganate (KMnO4, 99.9%); hydrogen chloride (HCl, 37%); hydrogen peroxide (H_2O_2, 30%); ethylene vinyl alcohol copolymer (EVOH) with 32% mol/ethylene (EVAL™ manufactured by Kuraray Co. Ltd.) were used in this study.

2.2. Preparation of graphene oxide (GO) nanosheets

GO was produced following a modified Hummers' method (Yoo et al., 2014). First, graphite (5 g) and potassium permanganate (15 g) were homogenized, then concentrated sulfuric acid (100 mL, 98%) was added by continuous mixing in an ice bath for 20 min. Next, the mixture was placed in a 90 °C water bath and maintained at that temperature for 60 min, followed by the slow addition of distilled water (400 mL) to keep the solution from effervescing. Then, a solution of hydrogen peroxide (30 mL) and distilled water (70 mL) (30/70%) was added and placed in a mechanical mixer for 2 h to facilitate the exfoliation of the graphitic domains. The mixture was washed repeatedly with dil. HCl, ethanol, and distilled water using a centrifuge until it reached a neutral pH. Subsequently, GO was added into dimethylformamide (DMF) (30 mL) and distilled water (70 mL) mixture and ultrasonicated using a high intensity ultrasonic device (20 kHz, and 450W/cm^2) for 2 h. After sonication, the aqueous solutions containing GO were frozen and freeze-dried for 24 h to obtain the GO powder.

2.3. Preparation of EVOH/GO flexible films

The EVOH/GO films were processed by twin-screw extrusion and extrusion blown film processing. The melting extrusion process was used to incorporate 0.1 to 0.3 wt % of GO in EVOH resin, using a twin-screw extruder Haake Rheomex P332 with 16 mm and L/D = 25 rate from Thermo-Scientific. The temperature profile was 182/192/197/197/205/205C °C and a screw speed of 30 rpm. The extrudates coming out of the extruder were cooled for better dimensional stability, pelletized by a pelletizer, dried again, and fed into extrusion blown film, single screw Haake Rheomex, L/D = 25 rate from Thermo-Scientific to obtain test samples of flexible film. The temperature profile used in the blow extrusion process of the EVOH films was 190/195/210/215/215/220 °C and screw speed was 30 rpm.

2.4. Electron beam irradiation

The flexible film samples (EVOH; EVOH/GO) were irradiated at 100 kGy and a dose rate of 22.3 kGy/s; using a 1.5 MeV, 2.81 mA, electron-beam accelerator, at room temperature, in the presence of air.

2.5. Characterization of GO

2.5.1. X-ray diffraction (XRD)

XRD patterns of graphite, GO nanosheet, and EVOH/GO flexible films were recorded on a siemens-d5000 diffractometer operated at 40 kv and 40 mA, with cukα radiation (λ = **15.4 Å).**

2.5.2. Thermogravimetric (TG) analysis

In this study, the TG analyses of the GO, RGO80, and RGO100 nanosheets were carried out using a Mettler Toledo TGA module "TGA/SDTA851e" from 30 to 1000 °C at a heating rate of 10 °C/min under nitrogen atmosphere (50 ml/min).

2.5.3. Attenuated total reflectance-Fourier transform infrared spectroscopy (ATR-FTIR)

ATR-FTIR spectra of the GO was recorded with a Nicolet Magna-IR 750 spectrometer equipped with a DGTS detector. Spectra were recorded accumulating 64 scans at 4 cm^{-1} resolution in Attenuated Total Reflection (ATR) mode using a single reflection diamond crystal.

2.5.4. Field emission scanning electron microscopy (FE-SEM)

FE-SEM analyses of the GO were conducted using a JEOL-JSM-6701 F microscope with an accelerating voltage of 1–30 kV, using EDS Thermo-Scientific Mod. Noran System Six software, in carbon sputtered samples.

2.5.5. Transmission electron microscopy (TEM)

TEM images of GO were obtained with a JEOL-1010 Field-Emission Transmission Electron Microscope, operating at an accelerating voltage of 80 kV.

2.6. Characterization of EVVOH/GO

2.6.1. X-ray diffraction (XRD)

XRD patterns of graphite, GO nanosheet and EVOH/GO flexible films were recorded on a Simens - D5000 diffractometer operated at 40 kv and 40 mA, with cukα radiation (λ = 15.4 å).

2.6.2. Oxygen transmission rate (OTR)

The OTR was determined based on ASTM D 3985–81, using an Oxtran 2/20 (Mocon Inc.) at test conditions of 23 °C, 0 and 90% relative humidity.

2.6.3. UV-VIS

UV/VIS spectra were obtained using a Shimadzu uv1601pc Spectrophotometer.

2.6.4. Mechanical tests

Tensile tests were determined using an Instron testing machine model 5564, according to ASTM D 882-91, to evaluate the mechanical behavior of the materials studied. Each value obtained represented the average of five samples.

2.6.5. Differential scanning calorimetry (DSC)

DSC analyses were performed with a Mettler Toledo DSC 822e from 25 to 250 °C at a heating rate of 10 °C/min under nitrogen atmosphere (50 ml/min). Two consecutive heating scans were conducted from 25 °C to 250 °C at 10 °C•min^{-1} with an intermediate cooling step at 10 °C•min^{-1}. DSC was carried out to obtain the melt temperature (Tm), melting enthalpy (ΔHm), and crystallinity percentage variation X_c (%) of non-irradiated and irradiated neat EVOH and EVOH/GO flexible films. The X_c is directly related to melting enthalpy (ΔHm) and was determined by the following equation:

$$X_C = (\Delta Hm/\Delta Hm^0\ (1 - W_f)) \times 100\% \quad [1]$$

Where:

ΔHm = melting enthalpy of sample
ΔHm^0 = melting enthalpy of EVOH assuming 100% crystallinity = 169.2 J/g
W_f = mass fraction of the GO in the flexible films

2.6.6. Thermogravimetric analysis (TG)

In this study, the TG analyses were done in a Mettler Toledo TGA module "TGA/SDTA851e" from 25 to 500 °C at a heating rate of 10 °C/min under nitrogen atmosphere (50 ml/min).

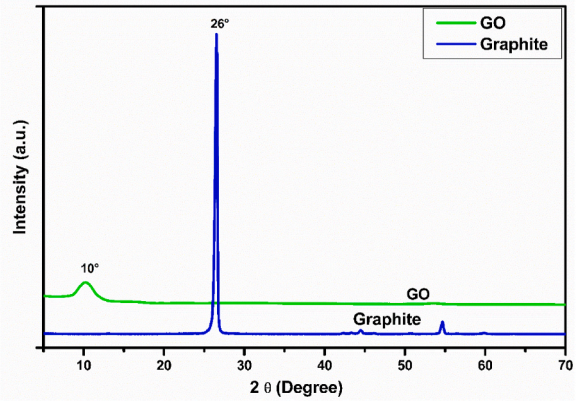

Fig. 1. XRD diffraction patterns for the graphite and graphene oxide sheets (GO).

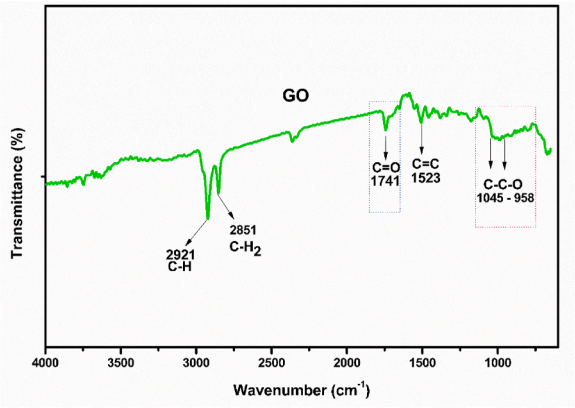

Fig. 2. ATR-FTIR spectra of GO in the range of 4000–600 cm^{-1}.

2.6.7. Attenuated total reflectance-Fourier transform infrared spectroscopy (ATR-FTIR)

ATR-FTIR spectra of the GO was recorded with a Nicolet Magna-IR 750 Spectrometer equipped with a DGTS detector. Spectra were recorded accumulating 64 scans at 4 cm^{-1} resolution in ATR mode using a single reflection diamond crystal.

2.6.8. Field emission scanning electron microscopy (FE-SEM)

FE-SEM of cryofractured samples under liquid nitrogen were conducted using a JEOL-JSM-6701 F microscope with an accelerating voltage of 1–30 KV, using EDS Thermo-Scientific Mod. Noran System Six software, on carbon sputtered samples.

3. Results and discussion

3.1. GO characterization results

3.1.1. XRD analysis results

XRD analysis of graphite and graphene oxide nanosheets (GO) are presented in Fig. 1. The diffraction peak for graphite powder was at 2θ = 26°, corresponding to the interlayer distance of 0.34 nm. After oxidation of graphite powder, the diffraction peak for graphene oxide was at 2θ = 10°, corresponding to the interlayer distance of 0.88 nm. The larger interlayer spacing of GO than graphite powder layers is due to the insertion of oxygen-containing functional groups between the layers. Similar findings have previously been reported (Huang et al., 2011; Wang et al., 2017; Emiru and Ayele, 2017).

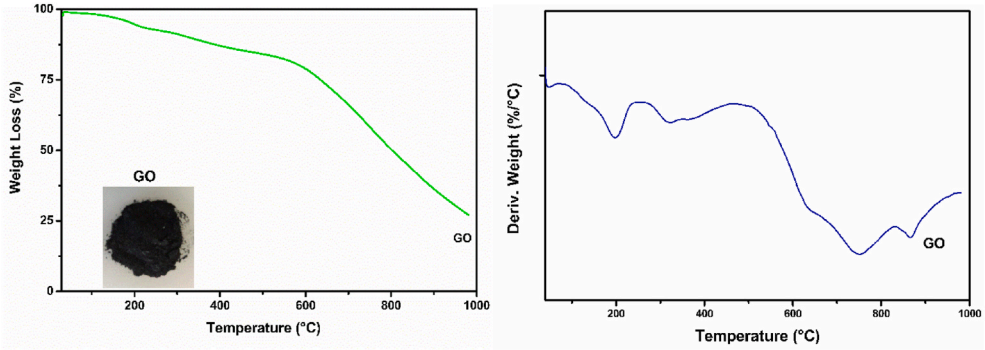

Fig. 3. TG (a) and (b) DTG curves of GO.

Table 1
Decomposition temperatures and weight loss of graphene oxide (GO).

Samples	Stage 1		Stage 2		Stage 3		T_{50} [b] (°C)
	T_{onset} (°C)	W.L. [a] (%)	T_{onset} (°C)	W.L. [a] (%)	T_{onset} (°C)	W.L. [a] (%)	
GO	42	6	235	10	543	28	800.6

[a] **W.L.** = Weight Loss.
[b] $\mathbf{T_{50}}$ = Degradation temperature at 50 wt % weight loss.

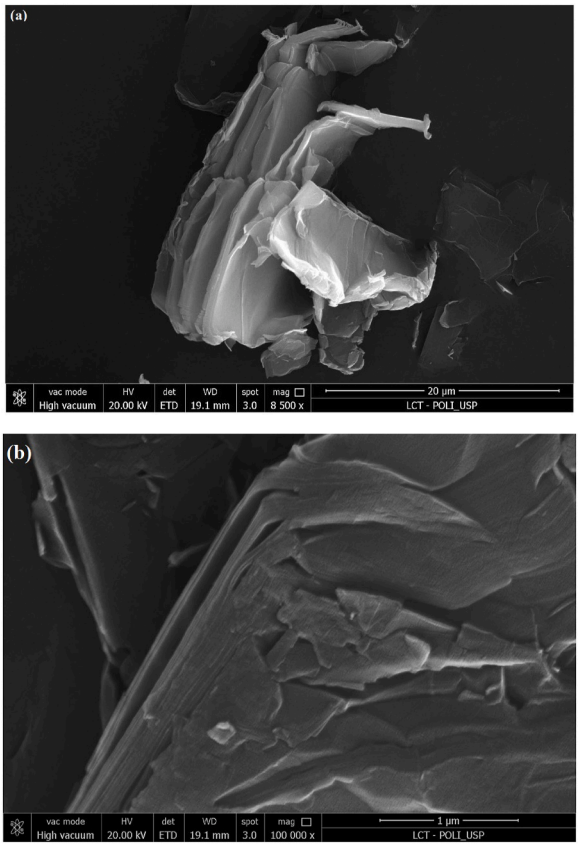

Fig. 4. FE-SEM images of GO with 8.500 × (4a) and with 100.000 × magnification (4b).

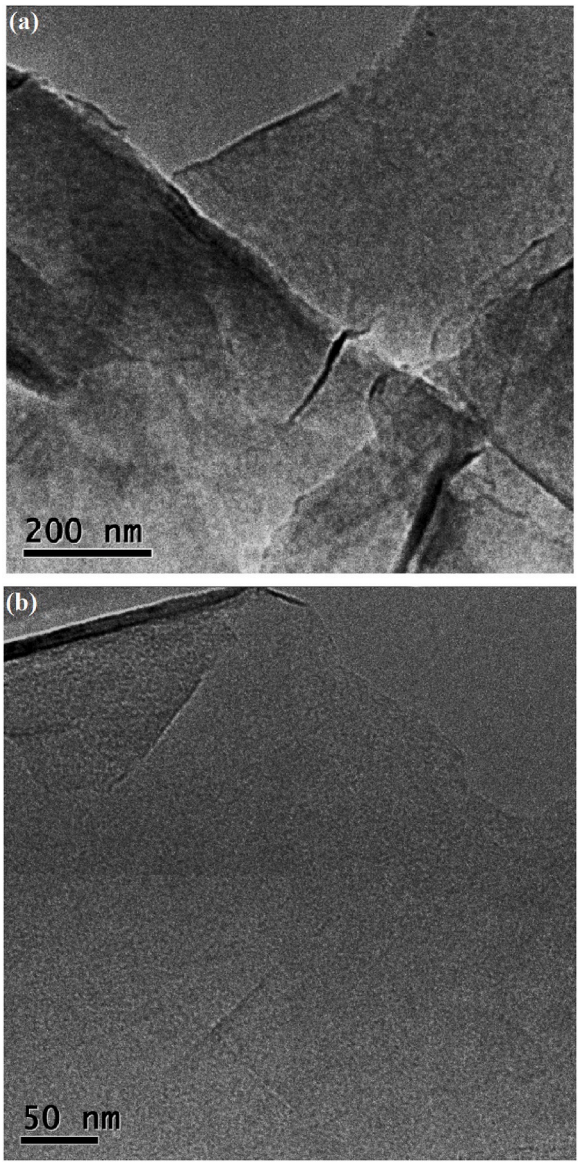

Fig. 5. TEM images of GO with 200 nm (5a) and with 50 nm magnification (5b).

3.1.2. *ATR-FTIR analysis results*

ATR-FTIR spectra of GO sheets are in Fig. 2. The intensity band observed at 1741 cm^{-1} is due to the mechanism of exfoliation mainly because of the expansion of CO_2 evolved in the interstices between the graphene sheets during rapid heating. The multiple peaks observed at 1500 to 958 cm^{-1} can be assigned to various functional groups, such as hydroxyl (1061 and 1393 cm^{-1}), epoxy groups (C–O–C) at 1233 cm^{-1}, carbonyl (C═O), and carboxylic in GO. The most intense bands are at

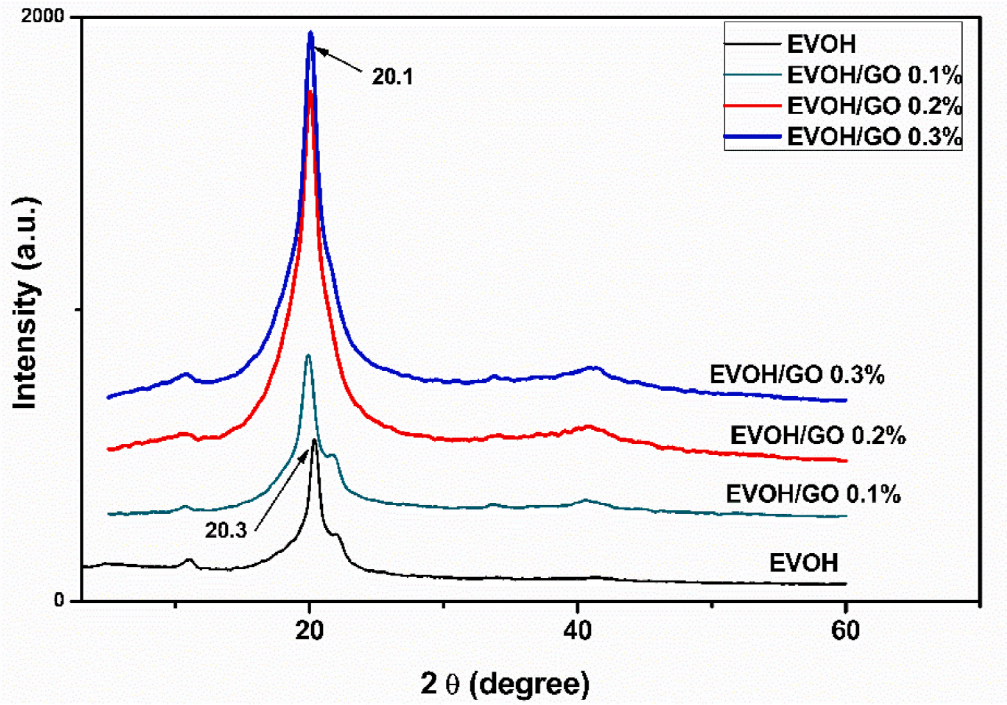

Fig. 6. XRD diffraction patterns for the neat EVOH and EVOH/GO flexible films.

approximately 2921 cm^{-1} and 2851 cm^{-1}, corresponding to the asymmetric vibration modes of elongation C–H and symmetrical C–H (CH_2) stretching, respectively (Huang et al., 2011; Wang et al., 2017; Emiru and Ayele, 2017; Meng and Park, 2012).

3.1.3. Thermogravimetric analysis results (TG)

Thermogravimetric analysis (TG) was used to investigate the thermal stability of the GO. Fig. 3 shows the TG (3a) and DTG curves (3b) for the GO. Three stages of degradation, in which the first is at the temperature range of 42–229 °C, could be due to the loss of moisture and corresponds to the decomposition of labile oxygen-containing functional groups. The second from 236 to 539 °C corresponds to the removal of more stable oxygen-containing functional groups. The last stage at a temperature range of 543–978 °C with a higher weight loss of about 50% at about 800 °C is associated with high-temperature pyrolysis of the carbon skeleton (El-Rehim and Tartour, 2018; Yang et al., 2014). This result indicates a higher thermal stability of GO and makes it suitable to incorporate into several polymer matrices, especially in EVOH matrix.

The decomposition temperatures and weight loss of GO are presented in Table 1.

3.1.4. FE-SEM analysis results

Fig. 4 shows FE-SEM micrographs of the GO surface with 8.500 × (4a) and with 100.000 × magnification (4b). Fig. 4a and b illustrate that GO had surface roughness with some aggregated domains and close stacking of sheets.

3.1.5. TEM analysis results

Fig. 5 presents the TEM images of GO with magnification of 200 nm (5a) and 50 nm (5b).

The image of GO nanosheet (5a; 5b) exhibits a flat and smooth surface with aggregated domains and transparent regions that are probably a monolayer of GO. Fig. 6a appears wrinkled with some folding regions, due to the formation and reconstruction of new chemical bonds on the single-layered carbon.

3.2. Characterization results of neat EVOH and EVOH/GO flexible films

3.2.1. XRD analysis results of neat EVOH and EVOH/GO flexible films

Fig. 6 shows the XRD patterns in the 2θ range of 2°–70° for neat EVOH and EVOH/GO flexible films. The characteristic peak of EVOH at

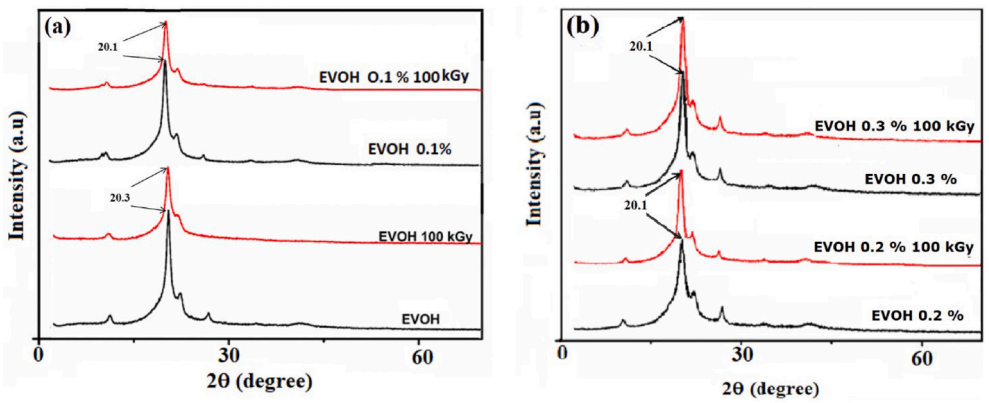

Fig. 7. XRD diffraction patterns for non-irradiated and irradiated flexible films; (a) neat EVOH and EVOH/GO 0.1%; (b) EVOH/GO 0.2–0.3%.

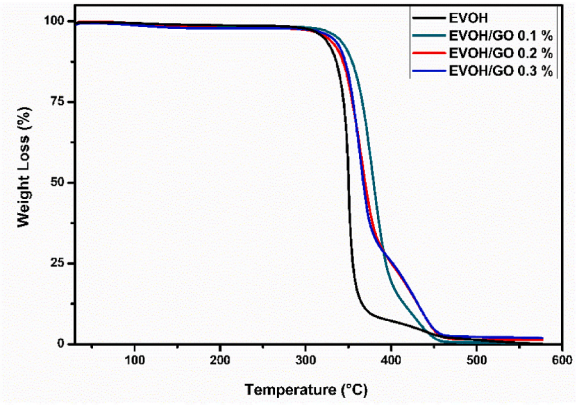

Fig. 8. TG thermograms of neat EVOH and EVOH/GO flexible films.

Table 2
Decomposition temperature and weight loss of neat EVOH and EVOH/GO films.

Flexible Films	T_{onset} (°C)	T_{max} (°C)	Total Weight Loss (%)
Neat EVOH	330	555	100
Neat EVOH IR	296.2	574	100
EVOH/GO (0.1) [a]	273.1	598	98.0
EVOH/GO IR (0.1) [a]	257.1	584	97.6
EVOH/GO (0.2) [b]	288.9	598	98.5
EVOH/GO IR (0.2) [b]	272.1	580	96.1
EVOH/GO (0.3) [c]	301.6	598	95.5
EVOH/GO IR (0.3) [c]	264.5	580	97.5

[a] EVOH/GO (99.9/0.1 wt %).
[b] EVOH/GO (99. 8/0.2 wt %).
[c] EVOH/GO (99.7/0.3 wt%).

20.3° is visible in the XRD patterns of neat EVOHVOH/GO (Kim and Choi, 2015; Meng and Park, 2012). A slight shift and formation of a thinner and higher peak at 2θ = 20.1° for EVOH/GO nanocomposites can also be seen in this figure (Kim and Lee, 2014). However, the characteristic peak of GO at 2θ = 10° for EVOH/GO was not observed, suggesting that some stacked layers remained, but a large part of GO sheets are intercalated between EVOH molecular chains (Zhan et al., 2021).

Fig. 7 shows the XRD patterns in the 2θ range of 2°–70° for non-irradiated and irradiated EVOH/GO flexible films. After irradiation of neat EVOH, no new peaks or peak shifts occurred, indicating stability in the lattice spacing, although a decrease in intensity of the characteristic peak of EVOH at 20.3° is clear. This decrease is attributed to the reduction of crystallinity degree, due to crosslinking caused by irradiation, which occurs preferentially in the amorphous region of EVOH, changing the molecular structure and hindering the growth of crystals (El-Saftawy et al., 2018; Moura et al., 2009; Nogueira Beatriz et al., 2011).

Figs. 6 and 7 illustrate that as the GO content was added from 0 to 0.3 wt %, a thinner and higher intensity peak at 2θ = 20.1° becomes visible for both non-irradiated and irradiated EVOH/GO. The addition of GO to EVOH clearly did not produce new peaks, but a shift from 2θ values of 20.3°–20.1°. This indicates that the intermolecular packaging order of neat EVOH decreased slightly due to the incorporation of GO, but it did not significantly alter or enhance the structural regularity of neat EVOH. After irradiation, a decrease in the intensity of the peak at 2θ = 20.1° was also observed for all the EVOH/GO nanocomposite films irradiated due to a decrease in the crystallinity degree in the EVOH because of crosslinking caused by irradiation (Kim et al., 2014a; Kim and Choi, 2015; El-Saftawy et al., 2018; Moura et al., 2009; Nogueira Beatriz et al., 2011).

3.2.2. TG analysis results of neat EVOH and EVOH/GO flexible films

Fig. 8 are the TG thermograms of the neat EVOH and EVOH/GO flexible films. TG of the composites showed a great difference in weight loss and in the onset degradation temperature from the neat EVOH. Changes in the thermal degradation temperature occurred in the irradiated EVOH and EVOH/GO samples. The decomposition temperature and weight loss of non-irradiated and irradiated EVOH/GO flexible films are provided in Table 2. The onset degradation temperatures of the EVOH/GO flexible films were less than for the neat EVOH due to the addition of GO nanosheets and e-beam irradiation. For all samples, the weight loss in the temperature ranging from 100 to 200 °C could be attributed to the absorbed water and the pyrolysis of oxygen-containing functional groups, such as –OH and –COOH (Yang et al., 2013a). The maximum temperature T_{max} increased due to GO addition and e-beam irradiation. This result confirms that the incorporation of GO into EVOH provided a significant improvement of the thermal stability of EVOH (Zhan et al., 2021; Kwon et al., 2013).

3.2.3. DSC analysis results of neat EVOH and EVOH/GO films

Table 3 shows the values of melting temperature (Tm), melting enthalpy (ΔHm), and crystallinity percentage of neat EVOH and EVOH/GO films. The crystallinity percentage of irradiated neat EVOH samples were not affected significantly in comparison to non-irradiated neat EVOH. It is very well known from the radiation effects in polymers that radiation-induced crosslinking occurs only in the amorphous phase of a semi-crystalline polymer; hence, the crystallinity of irradiated neat EVOH films remains almost the same.

Table 3 clearly demonstrates that the changes in melting temperature and enthalpy of EVOH were due to the addition of GO nanosheets. The incorporation of 0.1–0.3 wt % of GO nanosheets led to a significant reduction of the melting temperature and enthalpy of EVOH/GO and consequently in the crystallinity percentage of the original EVOH films. The reduction of melting enthalpy and consequently crystallinity percentage due to incorporation of GO nanosheets has also been observed and reported by various other authors (Yang et al., 2013a; Kim and Lee,

Table 3
DSC analysis results for neat EVOH and EVOH/GO flexible films.

EVOH Material	1° Heating Scans		2° Heating Scans		Crystallinity (Xc, %)
	Melting Temperature (Tm, °C)	Melting Enthalpy (ΔHm, Jg-1)	Melting Temperature (Tm, °C)	Melting Enthalpy (ΔHm, Jg-1)	
Neat EVOH	181.0	53,1	180.5	47	27.8
Neat EVOH IR	179.7	50.3	177.0	46.0	27.2
EVOH/GO 0.1[a]	178.9	53.8	174.5	36.0	21.5
EVOH/GO IR 0.1[a]	173.7	51.6	163.1	33.1	19.8
EVOH/GO 0.2 [b]	178.8	55.7	174.3	28.4	21.5
EVOH/GO IR 0.2[b]	174.3	55.6	160.6	24.1	17.1
EVOH/GO 0.3 [c]	180.9	58.5	174.0	21.1	14.7
EVOH/GO IR 0.3[c]	173.6	53.3	148.9	17.5	12.9

[a] EVOH/GO (99.9/0.1 wt %).
[b] EVOH/GO (99. 8/0.2 wt %).
[c] EVOH/GO (99.7/0.3 wt%).

Table 4
Oxygen transmission rate (OTR) results of neat EVOH and EVOH/GO flexible films.

Material	Thickness (μm)	23 °C Relative Humidity (RH)		OTR Factor of Increase (%)
		0 (%)	90 (%)	
Neat EVOH	40 ± 2	0.52 cc/ m^2.day	2.44 cc/ m^2.day	4.7
Neat EVOH IR	40 ± 2	0.43 cc/ m^2.day	1.74 cc/ m^2.day	4.0
EVOH/GO (0.1) [a]	40 ± 1.5	0.10 cc/ m^2.day	0.14 cc/ m^2.day	1.4
EVOH/GO IR (0.1) [a]	40 ± 1.5	0.08 cc/ m^2.day	0.10 cc/ m^2.day	1.25
EVOH/GO (0.2) [b]	30 ± 1.7	0.48 cc/ m^2.day	1.80 cc/ m^2.day	3.8
EVOH/GO IR (0.2) [b]	30 ± 1.7	0.36 cc/ m^2.day	1.30 cc/ m^2.day	3.6
EVOH/GO (0.3) [c]	35 ± 1.3	0.38 cc/ m^2.day	2.06 cc/ m^2.day	5.4
EVOH/GO IR (0.3) [c]	35 ± 1.3	0.32 cc/ m^2.day	1.42 cc/ m^2.day	4.4

[a] EVOH/GO (99.9/0.1 wt %).
[b] EVOH/GO (99. 8/0.2 wt %).
[c] EVOH/GO (99.7/0.3 wt%).

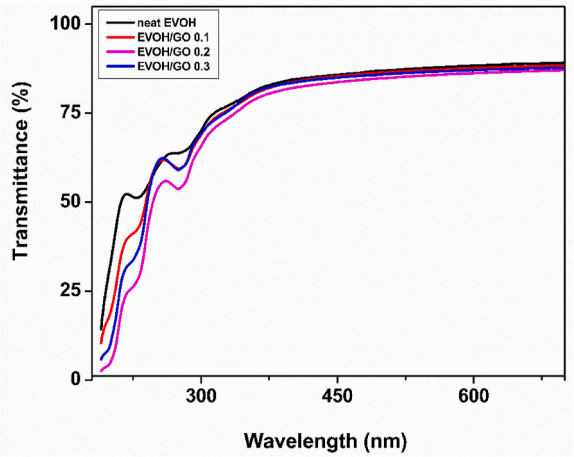

Fig. 9. UV-VIS transmittance spectra for the neat EVOH and EVOH/GO flexible films.

2014).

The irradiated EVOH/GO film samples presented a smaller melting temperature and enthalpy and crystallinity percentage than non-irradiated EVOH/GO films. According to Kim and Choi (2015), the reduction of Xc of EVOH with the incorporation of GO nanosheets is due to the strong interaction between the GO and EVOH, which confines the mobility of the EVOH chains close to the GO surface hindering the regular packing of the EVOH chains into crystal lattices (Yang et al., 2013a; Kim and Lee, 2014). The variation in Xc of EVOH observed in this work due to the addition of GO nanosheets is very important for EVOH/GO packaging applications, because in semi-crystalline polymers, like EVOH, the degree of crystallinity (Xc) and the crystalline structure induced by the crystallization process generally affect the gas-barrier performance as well as their physical and mechanical properties.

3.2.4. Analysis results for oxygen transmission rate (OTR) of neat EVOH and EVOH/GO films

Table 4 presents the oxygen transmission rate (OTR) of neat EVOH and EVOH/GO films measured at 23 °C and two different relative humidity test conditions (0 and 90%). With an incorporation of 0.1–0.3 wt % of GO nanosheets, the oxygen barrier properties of the EVOH/GO nanocomposite films in the 0% relative humidity test conditions were drastically improved, up to five orders of relative magnitude, compared to neat EVOH films. For EVOH/GO film with 0.1 and 0.2 wt % content of GO nanosheets, the increase of OTR in the 90% relative humidity test was less than for neat EVOH film. For irradiated EVOH/GO film samples, the oxygen barrier properties at 0% and 90% relative humidity test conditions were even less than non-irradiated EVOH/GO film samples. The reduction of melting enthalpy and consequently crystallinity percentage due to incorporation of GO nanosheets was also observed and reported. On the other hand, non-irradiated and irradiated EVOH/GO films with incorporation of 0.1 wt % GO nanosheets presented better oxygen barrier properties in both 0 and 90% relative humidity conditions and was even better for the irradiated samples.

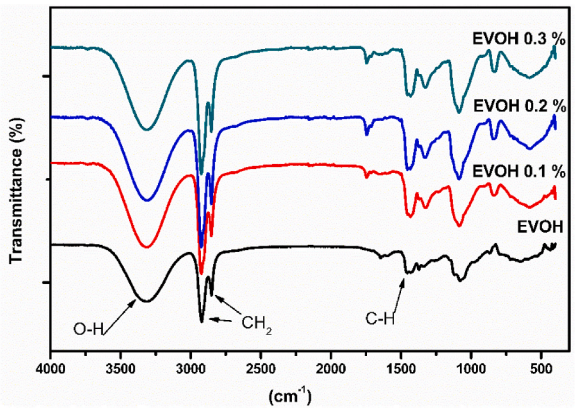

Fig. 10. ATR-FTIR spectra of EVOH and EVOH/GO in the range of 4000–600 cm^{-1}.

3.2.5. UV/VIS analysis results of neat EVOH and EVOH/GO films

Fig. 9 presents the UV-VIS transmittance spectra for the neat EVOH and EVOH/GO films. The addition of 0.1–0.3 wt % GO nanosheets led to a decrease in % transmittance at low wavelengths (195–350 nm) and to a very slight decrease at higher wavelengths (350–750 nm). At wavelengths within the UV range, light transmission is reduced with increased addition of GO nanosheets, which suggests that the UV barrier improved due to the incorporation of GO nanosheets. The high optical transparency is a significant requirement for the application of food packaging film because it can allow the visual identification of the condition of foods inside the film, such as freshness or spoilage. Therefore, the effect of graphene nanosheet incorporation on the variation of optical transparency of the EVOH/GO films was examined due to the possibility of its application as an oxygen barrier layer in multilayer food packaging structure. The neat EVOH and EVOH/GO films had a transparency with a light transmittance of around 87% in the entire visible light region. This result suggests that the incorporation of a small number of graphene nanosheets up to 0.3 wt % can yield a nanocomposite film with a good transparency to be utilized as food packaging films. For irradiated neat EVOH and EVOH/GO film samples, no significant changes were observed.

3.2.6. ATR-FTIR analysis results of neat EVOH and EVOH/GO films

Fig. 10 charts the ATR-FTIR-spectra of the neat EVOH and EVOH/GO films containing from 0.1 to 0.3 wt % of GO. EVOH and EVOH/GO spectra display the characteristic absorption peaks of EVOH at 2800–3000 cm^1 and 1300–1500 cm^{-1}, identified by symmetrical elongation chains (CH_2) and deformation bands (CH_3), respectively (Kim and Choi, 2015; Yang et al., 2013b, 2014; Zhan et al., 2021; Kwon et al., 2013; Kim et al., 2014b). The presence of absorption bands between 3100 and 3600 cm^{-1} indicates that O–H groups are present. There was a

Table 5
- Mechanical test results for neat EVOH and EVOH/GO flexible films.

Material	Thickness (μm)	Tensile strength at break (MPa)	Elongation at break (%)	Young's Modulus (MPa)
Neat EVOH	40 ± 2	35.9 ± 0.4	155.6 ± 9.6	257.7 ± 40.7
Neat EVOH IR	40 ± 2	36 ± 2	100 ± 6	258.4 ± 42.5
EVOH/GO 0.1	40 ± 1.5	31.4 ± 1.2	60.6 ± 7.4	351.7 ± 65.0
EVOH/GO IR 0.1	40 ± 1.5	46 ± 1	11 ± 1	515.3 ± 49.0
EVOH/GO 0.2	30 ± 1.7	25.9 ± 1.3	67.2 ± 3.7	297.9 ± 33.9
EVOH/ RGO IR 0.2	50 ± 1	41 ± 2	15 ± 1	471.6 ± 39.8
EVOH/GO 0.3	35 ± 1.3	23.1 ± 1.3	47.2 ± 1.8	227.4 ± 33.9
EVOH/ RGO IR 0.3	35 ± 1.3	50 ± 4	9 ± 0.3	492.2 ± 46.2

significant increase in the intensity of the peaks of the EVOH/GO spectra when compared to neat EVOH (Kim and Choi, 2015; Yang et al., 2013b, 2014; Zhan et al., 2021; Kwon et al., 2013; Kim et al., 2014b).

3.2.7. *Mechanical test results of neat EVOH and EVOH/GO flexible films*

The results presented in Table 5 from the mechanical tests show the average values calculated from the data obtained in tests for five test specimens, crosshead speed at 500 mm/min, with standard deviations less than 10% for all tests. The addition of GO nanosheets into EVOH caused a significant decrease in the original tensile strength and elongation at the break of EVOH film. However, an important increase in Young's modulus occurred for EVOH/GO films containing 0.1 and 0.2 wt % added GO. The Young's modulus increased with the increase up to 0.2% of GO incorporated into the matrix. The increase in Young's modulus was expected because of the high rigidity of GO due to its carbon-carbon sp^2 bonds. However, the tensile strength and elongation at break are more critical and dependent on the homogeneous distribution of GO in the matrix. The GO agglomerates can lead to rapid crack propagation and poor interfacial adhesion, which are the main factors associated with low nanocomposite strength. When the content of GO in the matrix increased to 0.3%, a reduction in Young's modulus was observed, due to the very bad dispersion of the GO in the EVOH matrix. The irradiated EVOH/GO film samples exhibited even higher tensile properties than non-irradiated EVOH/GO film samples (Yang et al., 2013b).

These results infer that e-beam radiation dose at 100 kGy used in this work can be considered economically feasible to apply commercially in EVOH/GO film. E-beam radiation at 100 kGy was a very convenient tool to create desirable effects on the properties of the film contributing to the production of a high-performance composite film based on EVOH resin for a variety of packaging applications, such as of food and electronic packaging. In addition, the gains in the mechanical properties and oxygen barrier produced by e-beam radiation dose at 100 kGy can reduce the film thickness, which leads to a reduction in the amount of raw material (EVOH resin). Considering the high price of EVOH resin in the international resin market, the radiation dose of 100 kGy could ultimately help reduce the final cost of producing the EVOH/GO, a high-performance composite film. Furthermore, commercial radiation applications on polymer materials using electron-beam accelerators (200

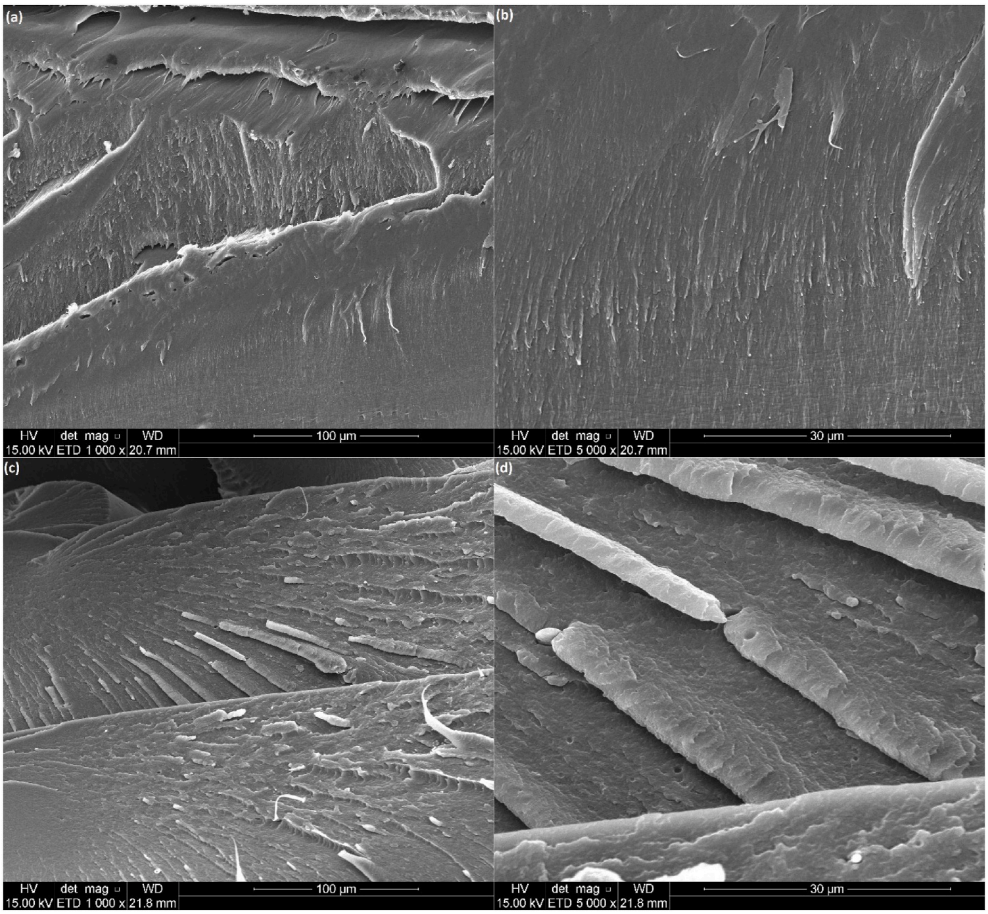

Fig. 11. FE-SEM images of neat EVOH and EVOH/GO, magnifications of 1000 × and 5000 × : neat EVOH (a,b); EVOH/GO(0.1% GO) (c,d).

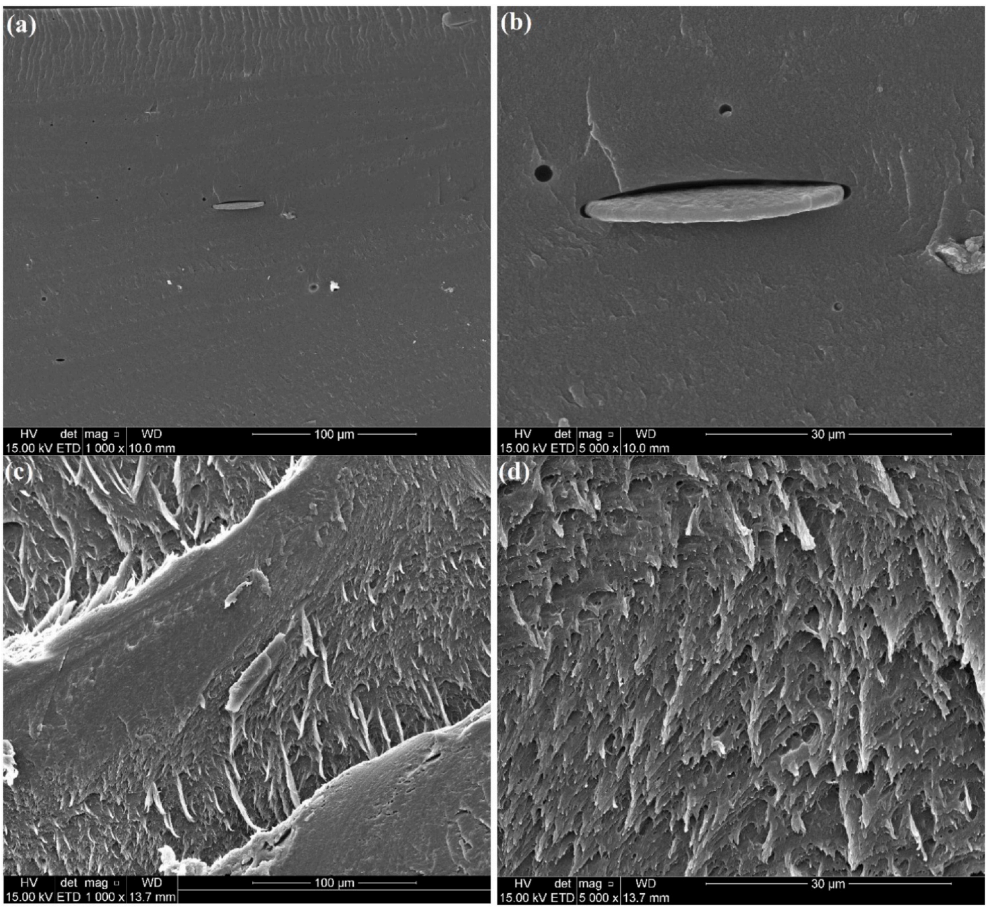

Fig. 12. FE-SEM images of EVOH/GO, magnifications of 1000 × and 5000 × : EVOH/GO 0.2% GO) (a,b); and 0.3% GO (c,d).

KeV to 10 MeV) are widely used the world over by wire/cable, heat shrinkable, surface curing, and other related industries, because of their ability to deliver high doses at large throughputs and thin products (Sarma, 2003; Sabharwal, 2013).

3.2.8. FE-SEM analysis results of neat EVOH and EVOH/GO flexible film

FE-SEM micrographs of cryofractured surfaces of the neat EVOH and EVOH/GO films were studied to understand the failure mechanisms and the possible interaction between GO nanosheets and EVOH resin. Fig. 11 contains FE-SEM micrographs of neat EVOH and EVOH/GO films in 1000 × and 5000 × magnifications, respectively, of neat EVOH (a,b), EVOH/GO with 0.1 wt % GO (c, d). Fig. 12 contains FE-SEM micrographs of EVOH/GO with 0.2 wt % GO (a, b), and EVOH/GO with 0.3 wt % (c, d). EVOH/GO with 0.1 wt % of GO presented a homogeneously dispersion of GO without any aggregation on the surface of the EVOH matrix. However, when 0.2 wt % of GO are added into the EVOH matrix, the arrangement of GO in EVOH became irregular, and there was some GO agglomeration. For EVOH/GO with 0.3 wt % GO, although GO aggregates cannot be seen on the FE-SEM micrographs of cryofractured surfaces, the corrugated surface suggests a non-homogeneous distribution of GO and its poor dispersion into the EVOH matrix.

4. Conclusions

This work investigated the effects of incorporating a small amount of graphene oxide into EVOH resin employing melt processing and e-beam irradiation on the morphology, optical transparency, mechanical resistance, and oxygen barrier of EVOH/GO nanocomposite films. Results showed that the incorporation of GO nanosheets in EVOH matrix obtained EVOH/GO flexible films with good transparency and light transmittance in the entire visible light spectra in comparison with EVOH flexible films as well as a better oxygen barrier. For irradiated EVOH/GO film samples, the oxygen barrier properties at 0% and 90% relative humidity test conditions were even less than non-irradiated EVOH/GO film samples. The tensile tests showed a significant decreasing in the original tensile strength and elongation at break of EVOH flexible film with increased amount of GO added, but an important increase in Young's modulus for flexible films containing 0.1 and 0.2 wt % of added GO was also observed. For irradiated EVOH/GO samples, the tensile properties based on this result indicate that the extent of exfoliation and dispersion state of the graphene oxide nanosheets in the EVOH matrix following e-beam irradiation are a significant factor for producing high-performance composite film based on EVOH resin for food packaging application. However, the methodology used to produce graphene oxide nanosheets is still a limiting factor for large production of EVOH/GO composite films.

Declaration of competing interest

The authors declare that they have no known competing financial interests or personal relationships that could have appeared to influence the work reported in this paper.

Acknowledgements

The authors wish to thank Intermarketing Brasil Comercial e Serviços Ltda and Kuraray Group for providing for raw materials, Fundacao de Amparo a Pesquisa do Estado de Sao Paulo (FAPESP, BRAZIL)/Process Number 2019/00862-9 for financial support.

References

Al-Jabareen, A., Al-Bustami, H., Harel, H., Marom, G., 2012. Improving the oxygen barrier properties of polyethylene terephthalate by graphite nanoplatelets. J. Appl. Polym. Sci. 128, 1534–1539.

Arora, A., Padua, G.W., 2010. Review: nanocomposites in food packaging. J. Food Sci. 75, 43–49.

Bumbudsanpharoke, N., Ko, S., 2015. Nano-food packaging: an overview of market, migration research, and safety regulations. J. Food Sci. 80, 910–923.

Cabedo, L., Lagaro, J.M., Cavaa, D., Saurab, J.J., Gimenez, E., 2006. The effect of ethylene content on the interaction between ethylene-vinyl alcohol copolymers and water - II: influence of water sorption on the mechanical properties of EVOH copolymers. Polym. Test. 25, 860–867.

Chen, H., Zhu, X., Liu, K., Wu, H., Zhang, M., Yan, C., 2020. Effect of electron beam irradiation on the properties of EVA/EPDM blends. Prog. Rubber Plast. Recycl. Technol. 36, 161–172. https://doi.org/10.1177/1477760619895005.

Coles, R., McDowell, D., Kirwan, M., 2003. J. Food Packaging Technology. Blackwell Publishing Ltd., Oxford, UK, ISBN 1-84127-221-3.

Cui, Y., Kundalwal, S.I., Kumar, S., 2016. Gas barrier performance of graphene/polymer nanocomposites. Carbon 98, 313–333.

El-Rehim, H.A.A., Tartour, A.R., 2018. Green synthesis of water dispersed graphene nanosheets using gamma radiation and natural capping agents. Radiat. Phys. Chem. 153, 208–213.

El-Saftawy, A.A., Ragheb, M.S., Zakhary, S.G., 2018. Electron beam irradiation impact on surface structure and wettability of ethylene-vinyl alcohol copolymer. Radiat. Phys. Chem. 147, 106–113 102. https://doi.org/10.1016/j.radphyschem.2018.02.001.

Emiru, T.F., Ayele, D.W., 2017. Controlled synthesis, characterization and reduction of graphene oxide: a convenient method for large scale production. Egypt. J. Basic Appl. Sci. 4, 74–79.

Huang, N., Huang, N.M., Lim, H.N., Chia, C.H., Yarmo, M.A., Muhamad, M.R., 2011. Simple room-temperature preparation of high-yield large-area graphene oxide. Int. J. Nanomed. 6, 3443–3448.

Huang, X., Qi, X., Boey, F., Zhang, H., 2012. Graphene-based composites. Chem. Soc. Rev. 41, 666–686.

Kim, S.W., Choi, H.M., 2015. Enhancement of thermal, mechanical, and barrier properties of ethylene vinyl alcohol copolymer by incorporation of graphene nanosheets: effect of functionalization of graphene oxide. High Perform. Polym. 27 (6), 694–704.

Kim, I.H., Jeong, Y.G., 2010. Polylactide/exfoliated graphite nanocomposites with enhanced thermal stability, mechanical modulus, and electrical conductivity. J. Polym. Sci., Part B: Polym. Phys. 48, 850–858.

Kim, H.M., Lee, H.S., 2014. Water and oxygen permeation through transparent ethylene vinyl alcohol/(graphene oxide) membranes. Carbon Lett. 15 (1), 50–56.

Kim, K.B., Sung, W.M., Park, H.J., Lee, Y.H., Han, S.H., 2004. Hydrophobic properties of ethylene–vinyl alcohol copolymer treated with plasma source ion implantation. J. Appl. Polym. Sci. 92 (4), 2069–2075.

Kim, S., Kang, P.H., Nho, Y.C., Yang, O.B., 2005. Effect of electron beam irradiation on physical properties of ultrahigh molecular weight polyethylene. J. Appl. Polym. Sci. 97, 103–116. https://doi.org/10.1002/app.21734.

Kim, D., Kwon, H., Seo, J., 2014a. EVOH nanocomposite films with enhanced barrier properties under high humidity conditions. Polym. Compos. 644–654.

Kim, D., Kwon, H., Seo, J., 2014b. EVOH nanocomposite films with enhanced barrier properties under high humidity conditions. Polym. Compos. 644–654.

Kucukpinar, E., Doruker, P., 2004. Effect of absorbed water on oxygen transport in EVOH matrices. A molecular dynamics study. Polymer 45, 3555–3564.

Kwon, H., Kim, D., Seo, J., Han, H., 2013. Enhanced moisture barrier films based on EVOH/exfoliated graphite (EGn) nanocomposite films by solution blending. Macromol. Res. 21 (9), 987–994.

Lasagabáster, A., Abad, M.J., Barral, L., Ares, A., Bouza, R., 2009. Application of FTIR spectroscopy to determine transport properties and water–polymer interactions in polypropylene (PP)/poly(ethylene-co-vinyl alcohol) (EVOH) blend films: effect of poly(ethylene-co-vinyl alcohol) content and water activity. Polymer 50, 2981–2989.

Marsh, K., Bugusu, B., 2007. Food packaging—roles, materials, and environmental issues. J. Food Sci. 72 (3), R39–R55.

Meng, L.Y., Park, S.J., 2012. Preparation and characterization of reduced graphene nanosheets via pre-exfoliation of graphite flakes. Bull. Kor. Chem. Soc. 33 (1), 209–214. https://doi.org/10.5012/bkcs.2012.33.1.209.

Mokwena, K.K., Tang, J., 2012. Ethylene vinyl alcohol: a review of barrier properties for packaging shelf stable foods. Crit. Rev. Food Sci. Nutr. 52, 640–650. https://doi.org/10.1080/10408398.2010.504903.

Mokwena, K.K., Tang, J., Dunne, C.P., Yang, T.C.S., Chow, E., 2009. Oxygen transmission of multilayer EVOH films after microwave sterilization. J. Food Eng. 92, 291–296.

Moura, E.A.B., Nogueira, B.R., Ortiz, A.V., 2009. Changes in physicochemical, morphological, and thermal properties of electron-beam irradiated ethylene-vinyl alcohol copolymer (EVOH) as a function of radiation dose. In: International Topical Meeting on Nuclear Research Applications and Utilization of Accelerators. May, Vienna, Austria, pp. 4–8.

Nogueira, Beatriz, R., Martinz, João, F.T., Oliveira, Rene, R., Moura, Esperidiana, A.B., 2011. Crystallinity changes of electron-beam irradiated ethylene-vinyl alcohol copolymer (EVOH) as a function of radiation dose. In: Proceedings of International Nuclear Atlantic Conference INAC, Belo Horizonte, MG. Brazil, 24–28 October.

Oliveira, Vitor M., Ortiz, Angel V., Del Mastro, Nélida, L., Moura, Esperidiana A.B., 2009. The influence of electron-beam irradiation on some mechanical properties of commercial multilayer flexible packaging materials. Radiat. Phys. Chem. 78, 553–555. https://doi.org/10.1016/j.radphyschem.2009.03.041.

Pramanik, N.K., Haldar, R.S., Niyogi, U.K., Alam, M.S., 2014. Development of an advanced engineering polymer from the modification of nylon 66 by e-beam irradiation. Defence Sci. J. 64, 281–289. https://doi.org/10.14429/dsj.64.7328.

Raheem, D., 2013. Application of plastics and paper as food packaging materials? An overview. Emir. J. Food Agric. 25 (3), 177–188. https://doi.org/10.9755/ejfa.v25i3.11509.

Riganakos, K.A., Koller, W.D., Ehlermann, D.A.E., Bauer, B., Kontominas, M.G., 1999. Effects of ionizing radiation on properties of monolayer and multilayer flexible food packaging materials. Radiat. Phys. Chem. 54, 527±540.

Sabharwal, S., 2013. Electron beam irradiation applications. In: Proceedings of PAC2013, vols. 745–748, ISBN 978-3-95450-138-0. Pasadena, CA USA.

Santana, J.G., Ortiz, A., Oliveira, R.R., Rangari, V.K., Güven, O., Moura, E.A.B., 2017. Mechanical, Thermal, morphology and barrier properties of flexible film based on polyethylene-ethylene vinyl alcohol blend reinforced with graphene oxide. In: The Minerals, Metals & Materials Series, 1ed. Springer International Publishing, Cham, Switzerland, pp. 49–57.

Sarma, K.S.S., 2003. Prospects and development of radiation technologies in developing countries. In: emerging applications of radiation processing, 14-20. In: Proceedings of a Technical Meeting. IAEA, Vienna (IAEA-TECDOC-13860, April 28–30.

Wang, H., Niu, B., Chen, M., Hao, L., Cao, X., Jiang, S., 2017. Facile layer-by-layer assembly to construct methoxybenzene group functionalized graphene/poly (ethylene-co-vinyl alcohol) barrier films under parallel electric field. Mater. Des. 118, 226–232.

Yang, J., Bai, L., Feng, G., Yang, X., Lv, M., Hu, C.Z.H., Wang, X., 2013a. Thermal reduced graphene based poly(ethylene vinyl alcohol) nanocomposites: enhanced mechanical properties, gas barrier, water resistance, and thermal stability. Ind. Eng. Chem. Res. 52, 16745–16754.

Yang, J., Bai, L., Feng, G., Yang, X., Lv, M., Zhang, C., Hu, H., Wang, X., 2013b. Thermal reduced graphene based poly(ethylene vinyl alcohol) nanocomposites: enhanced mechanical properties, gas barrier, water resistance, and thermal stability. Ind. Eng. Chem. Res. 52, 16745–16754.

Yang, H., Li, H., Zhai, J., Sun, L., Yu, H., 2014. Simple synthesis of graphene oxide using ultrasonic cleaner from expanded graphite. Ind. Eng. Chem. Res. 53 (46), 17878–17883.

Yoo, B., Shin, H., Yoon, H., Park, H., 2014. Graphene and graphene oxide and their uses in barrier polymers. J. Appl. Polym. Sci. 131, 39628 https://doi.org/10.1002/app.39628.

Zhan, Y., Meng, Y., Li, Y., Zhang, C., Xie, Q., Wei, S., Lavorgna, M., Chen, Z., 2021. Poly (vinyl alcohol)/reduced graphene oxide multilayered coatings: the effect of filler content on gas barrier and surface resistivity properties. Compos. Commun. 24, 100670.